Classical Axis-Displaced Dual-Reflector Antennas for Omnidirectional Coverage

Fernando José da Silva Moreira, *Member, IEEE,* and José Ricardo Bergmann, *Member, IEEE*

***Abstract*—The aim of this work is to discuss the synthesis and performance of classical dual-reflector antennas suited for an omnidirectional coverage. The reflector arrangements are axially symmetric with surfaces of revolution generated by axis-displaced conic sections, established from geometrical-optics (GO) standpoints to achieve omnidirectional radiation characteristics. Closed-form equations are derived for the design of all possible reflector configurations. The vector GO aperture field is also obtained, yielding an approximate analysis by the aperture method. Some pertinent geometrical characteristics and efficiency curves are then presented and discussed for several antenna configurations fed by transverse electromagnetic coaxial horns (for vertical polarization). A practical antenna design is conducted and analyzed by the method-of-moments technique, demonstrating the accuracy of the efficiency analysis yield by the aperture method for moderately large antenna apertures.**

***Index Terms*—Multireflector antennas, omnidirectional antennas, reflector antennas.**

I. Introduction

REFLECTOR antennas are typically employed in microwave and millimeter-wave point-to-point radio links. They also appear on board satellites for communication services demanding point-to-multipoint coverages [1]. Such applications illustrate the use of directive configurations, but (single) reflector antennas have also been designed in the past with omnidirectional radiation characteristics [2], [3]. In recent years, the interest on the design of reflector antennas for omnidirectional coverage has been renewed [4]–[10], essentially because of their inherent geometrical properties, which ultimately allows their use for the transmission and reception of wideband signals.

A dual-reflector antenna for omnidirectional coverage was presented in [4], where a Cassegrain-based axially-symmetric configuration was shaped for a prescribed radiation pattern in the elevation plane. A TM_{01} conical horn was employed to yield the desired circularly symmetric excitation and vertical polarization. Afterwards, a dual-reflector system with a paraboloidal subreflector and a conical main-reflector, fed by a transverse electromagnetic (TEM) coaxial horn, was investigated in [5]. In this work the reflector surfaces were not shaped (and the feed is a different one), but the configuration is essentially that of [4]. Similar configurations were also investigated in [6]–[8].

Recently, a novel dual-reflector arrangement for omnidirectional coverage based on an axis-displaced ellipse (ADE) configuration was presented [10]. Due to the inversion of the feed radiation provided by the ADE subreflector, the feed main-beam radiation can be, in principle, directed away from the feed aperture, thus reducing the overall return loss. Also, the ADE-based antenna has different geometrical aspects when compared to its Cassegrain-based counterpart, enabling a second choice for antenna designers.

Actually, such configurations are examples of dual-reflectors antennas generated by axis-displaced conic sections (classical configurations, without any shaping). Both reflectors (surfaces of revolution) are set from geometrical optics (GO) principles to transform the rays emanating from the principal focus into a bundle of rays perpendicular to the main-reflector aperture. It was demonstrated in [11] that such antennas can be classified into four different families. Although the work in [11] was devoted to directive axially-symmetric dual-reflector antennas, the same classification applies for the present omnidirectional arrangements, as their geometrical features are very much similar to each other. So, the main objective of the present work is to present closed-form design equations for the four possible classical omnidirectional dual-reflector configurations, in a unified way. To our best knowledge, such design equations are not available in the open literature. Besides, they provide useful tools for the antenna synthesis, even to initialize a shaping procedure.

The work is conducted as follows. In Section II the basic geometrical aspects of all possible classical dual-reflector configurations are presented and discussed, together with closed-form equations for the antenna synthesis based on GO. Some geometrical features are then illustrated and discussed in Section III, yielding some insights for the achievement of compact geometries. The vector GO aperture field is established in Section IV, enabling an approximate analysis of the antennas by the aperture method. Such analysis is then applied in Section V for a large number of classical dual-reflector configurations (fed by TEM coaxial horns), yielding aperture-efficiency curves and, consequently, the establishment of highly-efficient configurations. In Section VI a case study is conducted in order to illustrate the capabilities of the present formulation. The antenna is further analyzed by the method-of-moments technique in order to estimate limits for the applicability of the proposed aperture-method analysis. Finally, some remarks and conclusions are made in Section VII.

Manuscript received June 18, 2004; revised November 3, 2004. This work was supported in part by the CNPq under Covenant PRONEX 664041/1996-S and Projects 462669/00-9, 470495/2001-4, and 551990/2002-2, and in part by FAPEMIG under Project TEC 659/98.

F. J. S. Moreira is with the Department of Electronics Engineering, Federal University of Minas Gerais, 31270-901 Belo Horizonte, Brazil (e-mail: fernandomoreira@ufmg.br).

J. R. Bergmann is with the Center for Telecommunications Studies, Catholic University, 22453-900 Rio de Janeiro, Brazil.

Digital Object Identifier 10.1109/TAP.2005.854560

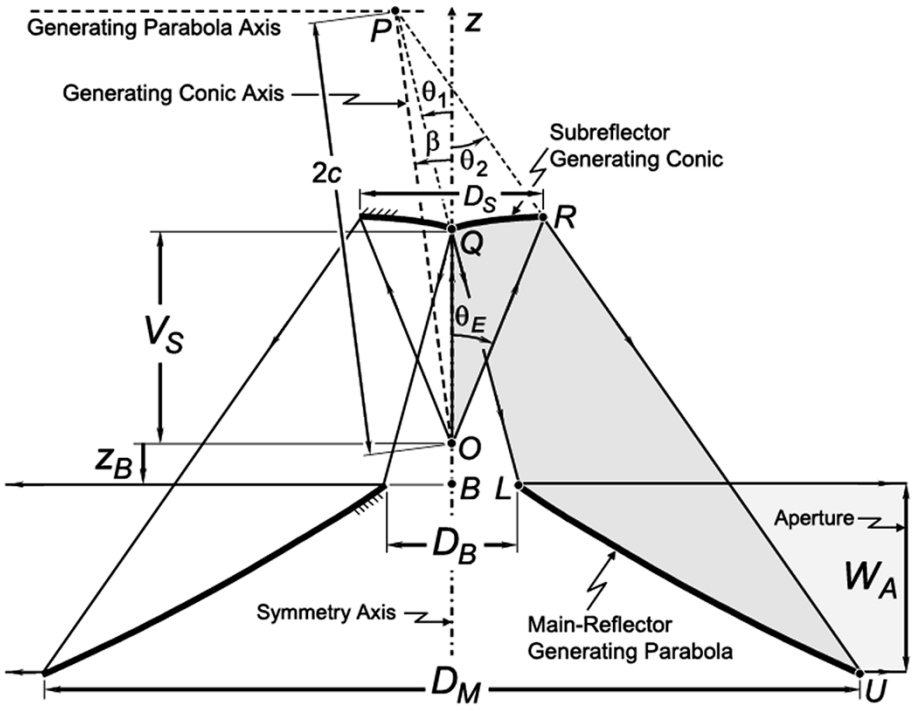

Fig. 1. Basic geometrical parameters of an OADC.

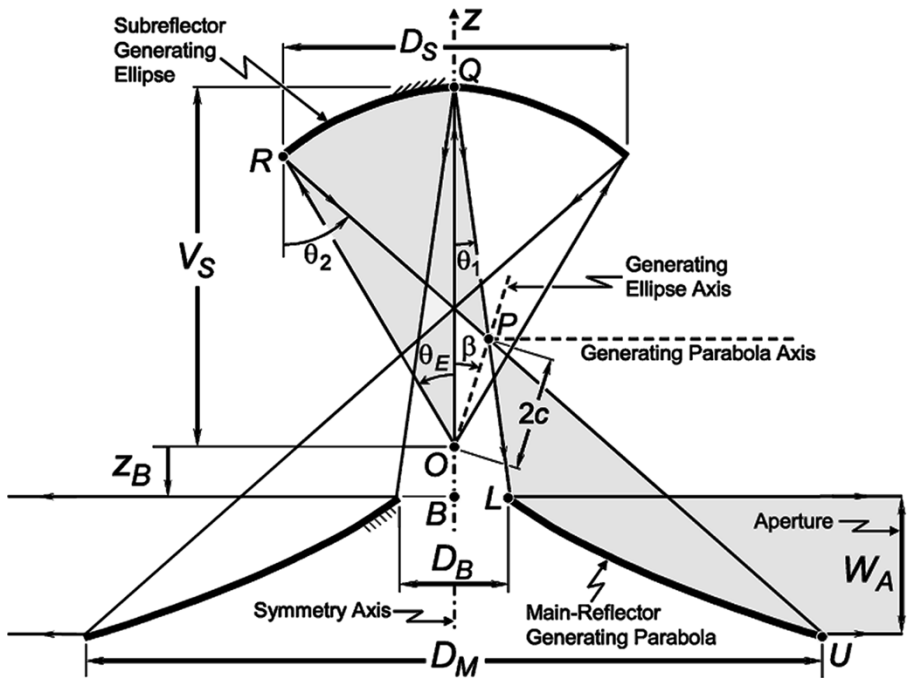

Fig. 2. Basic geometrical parameters of an OADG.

II. Synthesis of Classical Omnidirectional Dual-Reflector Antennas

The study to be conducted is based on [11], where directive classical axially-symmetric dual-reflector antennas, with surfaces of revolution generated by conic sections, were uniformly investigated. It was demonstrated that such antennas are classified in four distinct families, namely axis-displaced Cassegrain (ADC), axis-displaced Gregorian (ADG), axis-displaced ellipse (ADE), and axis-displaced hyperbola (ADH). The theory developed in [11] can be extended to yield omnidirectional arrangements. This is accomplished by tilting the axis of the main-reflector by 90°, imposing a right angle between the rays that leave the main reflector and the symmetry axis of the dual-reflector system. This establishes a cylindrical aperture for the antenna. Hereinafter, the antennas will be defined as omnidirectional ADC (OADC), ADG (OADG), ADE (OADE), and ADH (OADH). Their geometries are depicted in Figs. 1–4.

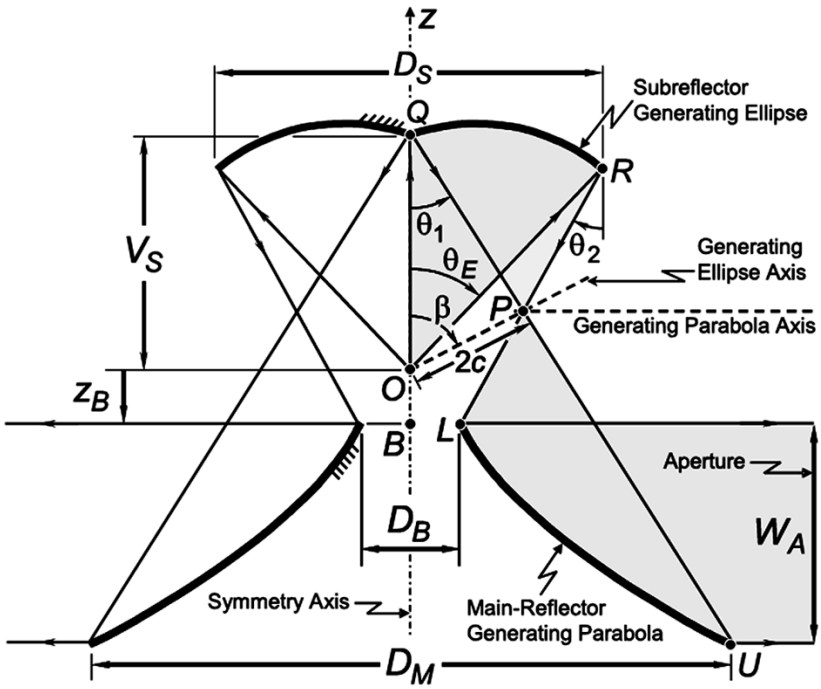

Fig. 3. Basic geometrical parameters of an OADE.

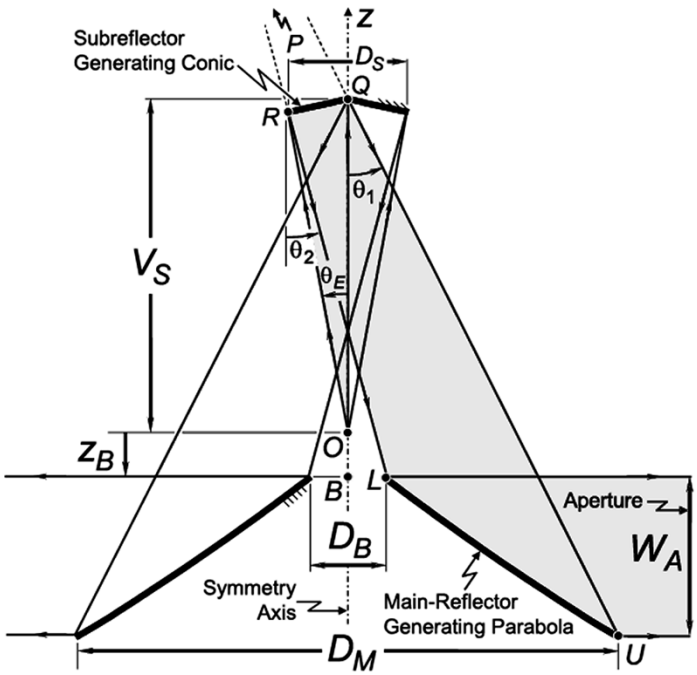

Fig. 4. Basic geometrical parameters of an OADH.

The main difference among these antennas is the location of the caustics of the astigmatic wavefront reflected by the subreflector. One is a ring caustic defined by P (see Figs. 1–4), which is the common focus of both generating conics—the other focus of the subreflector generating conic is O, which defines the principal focus of the dual-reflector system. The second is the line caustic defined by the intersection of the ray reflected by the subreflector with the symmetry axis. For the OADC and OADH (OADG and OADE) the ring caustic is virtual (real). For the OADC and OADG (OADE and OADH) the line caustic is virtual (real). The presence of a single real caustic between the reflectors (which occurs for the OADE and OADH) provides the inversion of the feed radiation at the antenna cylindrical aperture (in the elevation plane, as depicted in Figs. 3 and 4).

Both OADG and OADE have subreflectors generated by ellipses and a convex main-reflector generating parabola, while for the OADC and OADH the subreflectors can be generated by any conic section and the generating parabola can be either concave or convex, depending on the location of P. It is interesting

to note that the so called *mushroom* antenna [5] is actually a particular case of the OADC with $D_B = 0$ (see Fig. 1), which provides a paraboloidal subreflector and a conical main reflector with an internal semi-angle of 45°.

Following the concepts in [11], five independent input parameters are necessary and sufficient to uniquely define a classical axially-symmetric dual-reflector configuration. For the omnidirectional arrangements at hand they will be the following (see Figs. 1–4): the width (W_A) of the antenna cylindrical aperture, the diameters of the rim (D_M) and central hole (D_B) of the main reflector, the distance (V_S) between the principal focus O and the subreflector vertex Q, and the z-coordinate (z_B) of B (the center of the main-reflector central hole). Note that the focus O will always be assumed at the origin. The input parameters D_B, V_S, and z_B are useful for the appropriate fed access to the principal focus and to its relative position with respect to the subreflector. For instance, in OADE configurations z_B (which is negative, according to Fig. 3) can be decreased to reduce the subreflector back-scattering toward the horn's aperture and, consequently, the corresponding return loss. The other parameters (W_A and D_M) basically control the overall antenna dimensions and radiation characteristics (together with the feed illumination).

To simplify the design procedure, two auxiliary angles are adopted: θ_1 and θ_2, as illustrated in Figs. 1–4. Note that θ_1 is always related to the principal optical path, which departs from O along the symmetry axis. Also, any angle in Figs. 1–4 is hereinafter considered positive (negative) if it has a clockwise (counterclockwise) orientation. Such definitions are necessary for a uniform description of the generating conics [11].

A. Classical OADC and OADG Designs

It turns out that the procedure is the same for both OADC and OADG. The closed-form equations are obtained with the help of Figs. 1 and 2. From the triangle OQL (ΔOQL)

$$\tan\theta_1 = \frac{-D_B}{2(V_S - z_B)} \tag{1}$$

which sets the value of θ_1. Then, one can show from the equation of the main-reflector generating parabola that

$$\frac{D_M - D_B}{2W_A} = \frac{1 - \tan(\theta_1/2)\tan(\theta_2/2)}{[1 + \tan(\theta_1/2)][1 + \tan(\theta_2/2)]} \tag{2}$$

from which one immediately obtains θ_2. The parabola's equation also provides the corresponding focal length

$$F = \frac{W_A[1 + \tan(\theta_1/2)][1 + \tan(\theta_2/2)]}{4[\tan(\theta_1/2) - \tan(\theta_2/2)]}. \tag{3}$$

The interfocal distance $(2c = |\overline{OP}|)$ and the axial tilt angle (β) of the subreflector generating conic are next determined by applying the sine law to ΔOPQ and ΔOPU. Doing so

$$2c\sin(\beta - \theta_1) = -V_S \sin\theta_1 \tag{4}$$

$$2c\sin(\beta - \theta_2) = (W_A - z_B)\sin\theta_2 + (D_M/2)\cos\theta_2. \tag{5}$$

From (4) and (5) one then obtains

$$2c\sin\beta = \left[\frac{D_M + 2(V_S + W_A - z_B)\tan\theta_2}{2(\tan\theta_1 - \tan\theta_2)}\right]\tan\theta_1 \tag{6}$$

$$2c\cos\beta = \frac{D_M + 2V_S\tan\theta_1 + 2(W_A - z_B)\tan\theta_2}{2(\tan\theta_1 - \tan\theta_2)} \tag{7}$$

and, consequently, the values of $2c$ and β. Finally, the eccentricity (e) of the subreflector conic is given by the corresponding conic equation. From the principal optical path

$$\frac{2c}{e} = V_S - \frac{2c\sin\beta}{\sin\theta_1}. \tag{8}$$

At this point the reflector surfaces are completely and uniquely determined. However, two other geometrical parameters are useful in the analysis: the edge angle (θ_E) and rim diameter (D_S) of the subreflector. Both are determined by applying the sine law to ΔOPR in Figs. 1 and 2

$$\frac{2c}{\sin(\theta_E - \theta_2)} = \frac{|D_S/\sin\theta_E|}{2\sin(\beta - \theta_2)} = \frac{(4c/e) - |D_S/\sin\theta_E|}{2\sin(\beta - \theta_E)} \tag{9}$$

from which, together with (4) and (8), one obtains

$$\tan\left(\frac{\theta_E}{2}\right) = \frac{\tan(\theta_2/2) - \tan(\theta_1/2)}{1 - [2\cot\beta + \tan(\theta_2/2)]\tan(\theta_1/2)} \tag{10}$$

$$D_S = \frac{4c|\sin\theta_E|\sin(\beta - \theta_2)}{\sin(\theta_E - \theta_2)}. \tag{11}$$

Together with the input parameters, D_S is important in the determination of compact dual-reflector arrangements. The edge angle θ_E is intimately related to the illumination efficiency of the reflectors. Besides, θ_E defines if the present configuration is an OADC (when $\theta_E > 0$) or an OADG ($\theta_E < 0$). This feature will permit the uniform investigation of both antennas.

B. Classical OADE and OADH Designs

The procedure closely follows the previous one. The difference is in the inversion between θ_1 and θ_2 with respect to the parabola extremes (L and U in Figs. 1–4). Now, with the help of Figs. 3 and 4, ΔOQU provides θ_1 from

$$\tan\theta_1 = \frac{-D_M}{2(V_S - z_B + W_A)}. \tag{12}$$

Next, the equation of the main-reflector generating parabola is applied to obtain θ_2 and F. The former is still given by (2). However, due to the inversion between θ_1 and θ_2, (3) must have its sign changed for the present antennas

$$F = \frac{-W_A[1 + \tan(\theta_1/2)][1 + \tan(\theta_2/2)]}{4[\tan(\theta_1/2) - \tan(\theta_2/2)]}. \tag{13}$$

The subreflector conic parameters $2c$ and β are obtained by applying the sine law to ΔOPQ, to obtain (4) once more, and to ΔOPL, to obtain

$$2c\sin(\beta - \theta_2) = (D_B/2)\cos\theta_2 - z_B\sin\theta_2. \tag{14}$$

Then, from (4) and (14)

$$2c\sin\beta = \left[\frac{D_B + 2(V_S - z_B)\tan\theta_2}{2(\tan\theta_1 - \tan\theta_2)}\right]\tan\theta_1 \qquad (15)$$

$$2c\cos\beta = \frac{D_B + 2V_S\tan\theta_1 - 2z_B\tan\theta_2}{2(\tan\theta_1 - \tan\theta_2)}. \qquad (16)$$

The eccentricity of the subreflector generating conic is still obtained from (8), now with $2c\sin\beta$ given by (15). Finally, θ_E and D_S are still determined from (10) and (11), respectively. Furthermore, the antenna configuration is an OADE (OADH) if θ_E is positive (negative).

III. Geometrical Features for Compact Arrangements

To illustrate some important features of the classical omnidirectional configurations, three geometrical characteristics are investigated: the edge angle (θ_E) and rim diameter (D_S) of the subreflector and the antenna volume (defined as the volume of the cylinder that circumscribes the dual-reflector system). Such parameters are relevant in the definition of compact dual-reflector arrangements. The cylindrical volume definition adopted here is subjective. For instance, smaller cylindrical volumes do not necessarily mean lighter antennas (that basically depends on D_M and D_S). In any event, the information in Figs. 5 and 6 provides insights of the overall dimensions for several classical omnidirectional configurations.

Some features specifically related to θ_E must be emphasized at this point. From Figs. 1–4, one can inspect that the antenna cylindrical aperture is (geometrically) blocked by the subreflector if $|\theta_E| > 90°$. Such cases are identified and removed from the analyses to follow. Also, as pointed out in Section II, the closed-form equations allow a uniform analysis of the OADC and OADG (OADE and OADH), which are identified according to the sign of θ_E in (10). So, in Figs. 5 and 6 (and others to follow) dashed lines indicate either $|\theta_E| = 90°$ (the limit for avoiding aperture blockage) or $\theta_E = 0°$ (separating the OADC from the OADG or the OADE from the OADH).

Figs. 5 and 6 illustrate the behavior of θ_E, D_S, and the volume for the OADC/OADG and OADE/OADH pairs, respectively, as functions of V_S and D_M. In these plots the values $W_A = 10\lambda, D_B = 2\lambda$, and $z_B = 0$ where arbitrarily set but aiming compact reflector arrangements. Note from Figs. 5(b) and 6(b) that, in general and for the OADC and OADE, D_S increases as D_M decreases (the opposite being for the OADG and OADH), which explains the apparently anomalous behavior of the volume contour plots in Figs. 5(c) and 6(c) whenever $D_S = D_M$. Consequently, the volume of the circumscribing cylinder will increase (decrease) with D_M if $D_M > D_S (D_M < D_S)$. The volume always increase with V_S, as expected. From these figures one also observes that the minimum cylindrical volume is achieved by the OADE when $D_M = D_S$ and $\theta_E = 90°$, while the OADG and OADH are not appropriate for compact arrangements. For the sake of comparison, Fig. 7 depicts scale views of the OADC and OADE with the lowest cylindrical volumes among those geometries considered in Figs. 5 and 6, respectively.

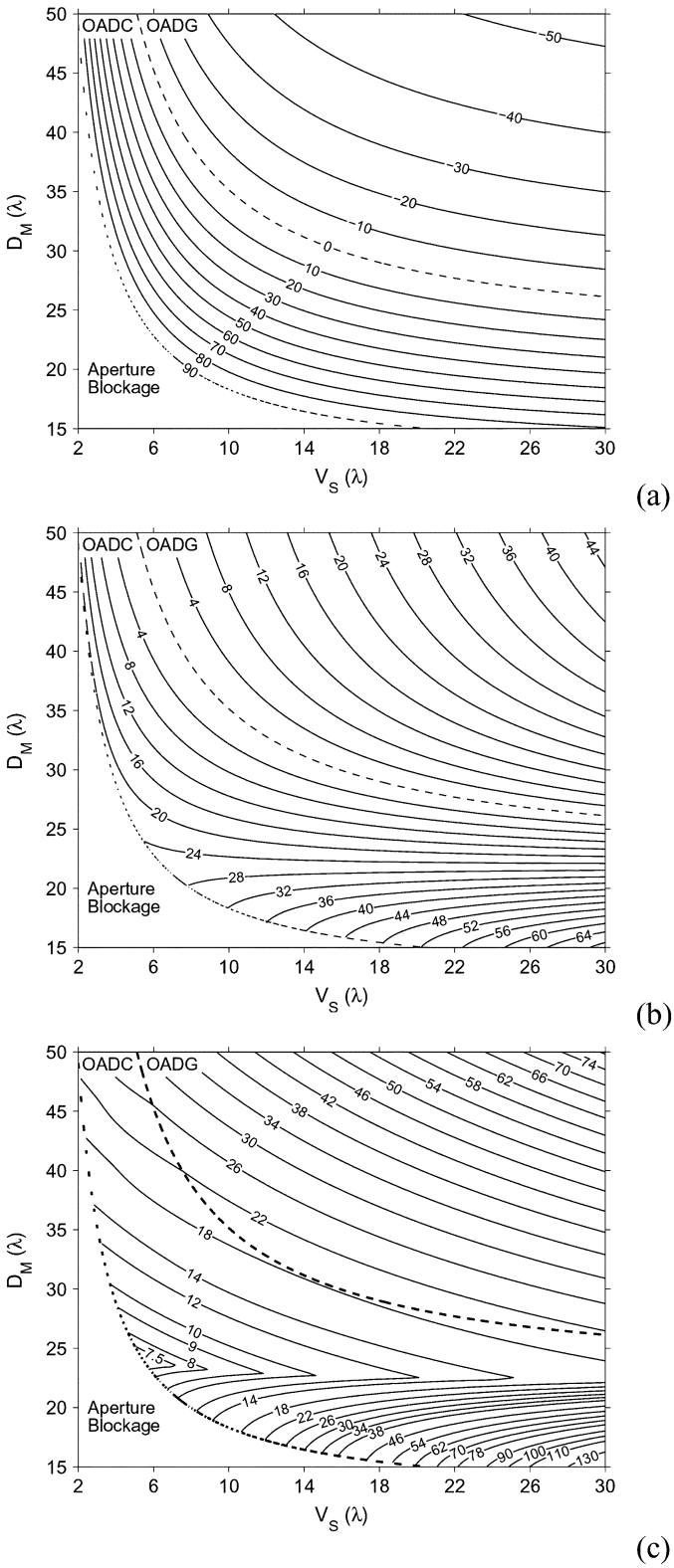

Fig. 5. Geometrical characteristics of the OADC and OADG as functions of V_S and D_M for $W_A = 10\lambda, D_B = 2\lambda$, and $z_B = 0$: (a) $\theta_E(°)$, (b) $D_S(\lambda)$, and (c) cylindrical volume $(\times 10^3\lambda^2)$.

IV. GO Aperture Field

Once the conic parameters $(F, 2c, e$, and $\beta)$ are determined from the closed-form equations presented in Section II, one has the necessary information to describe the surfaces of revolution

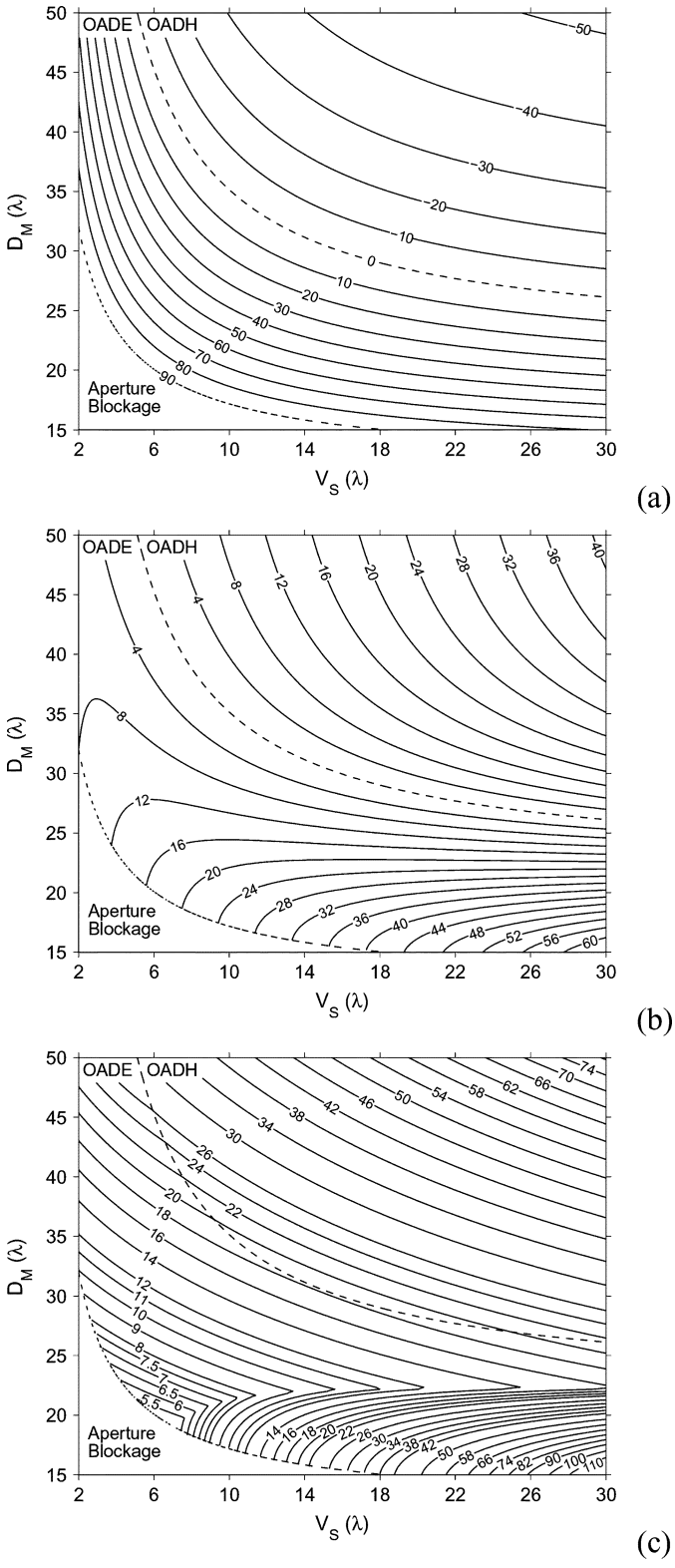

Fig. 6. Geometrical characteristics of the OADE and OADH as functions of V_S and D_M for $W_A = 10\lambda$, $D_B = 2\lambda$, and $z_B = 0$: (a) $\theta_E(^\circ)$, (b) $D_S(\lambda)$, and (c) cylindrical volume ($\times 10^3\lambda^2$).

of the dual-reflector system. The aperture limits (imposed by the finite reflector's dimensions) are specified by the input parameters W_A and z_B or, more appropriately, by θ_E, which limits the conical bundle of rays leaving O (as depicted in Fig. 8). So,

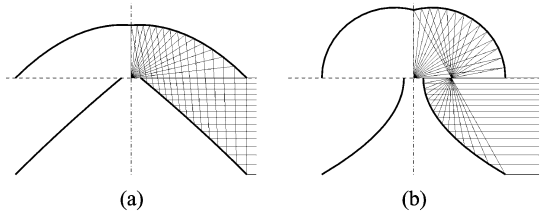

Fig. 7. Scale views of the (a) OADC ($D_M = 24\lambda$ and $V_S = 5.45\lambda$) and (b) OADE ($D_M = 19.04\lambda$ and $V_S = 7.05\lambda$) with minimum cylindrical volumes for $W_A = 10\lambda$, $D_B = 2\lambda$, and $z_B = 0$.

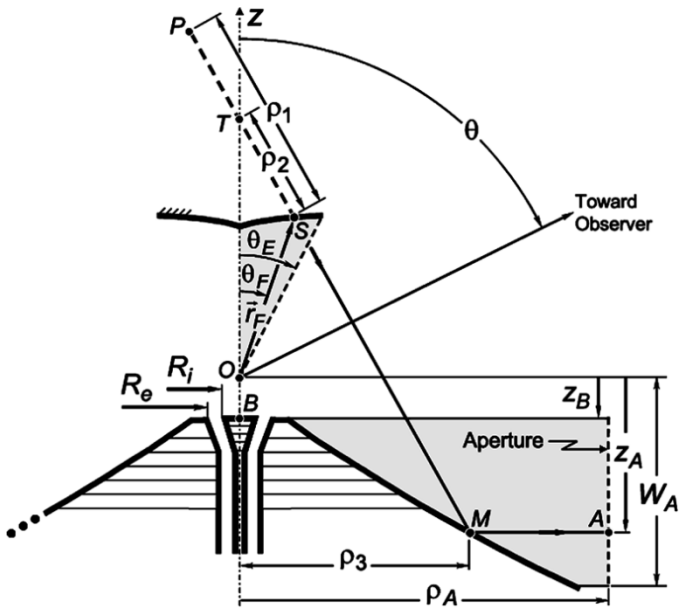

Fig. 8. Geometrical parameters for the attainment of the GO aperture field.

from the (usual) conic equations and for each (input) direction $\theta_F \leq |\theta_E|$ one then obtains the coordinates of all relevant points shown in Fig. 8. Due to the cylindrical nature of the GO aperture field, the aperture illumination efficiency is specified with respect to a uniformly illuminated cylindrical aperture with the same W_A and ρ_A (see Fig. 8). Consequently, ρ_A can be arbitrarily chosen, as the aperture's taper efficiency will not depend on it.

Following GO principles, the feed TEM spherical radiation emanating from O is arbitrarily represented as

$$\vec{E}_F(\vec{r}_F) = [F(\theta_F)\hat{\theta}_F + P(\theta_F)\hat{\phi}_F]\frac{e^{-jkr_F}}{r_F} \tag{17}$$

where r_F, θ_F, and ϕ_F are the usual spherical coordinates locating S, as depicted in Fig. 8. Due to the azimuthal symmetry and from GO principles [12], the TEM field at the aperture point A is represented by

$$\begin{aligned}\vec{E}_A(\vec{r}_A) &= \epsilon[-F(\theta_F)\hat{z} + P(\theta_F)\hat{\phi}]A_1A_2A_3e^{-jk\ell} \\ \vec{H}_A(\vec{r}_A) &= \frac{1}{\eta}\hat{\rho}\times\vec{E}_A(\vec{r}_A)\end{aligned} \tag{18}$$

where $\epsilon = 1(=-1)$ for the OADC and OADE (OADG and OADH), $\ell = |\overline{OS}| + |\overline{SM}| + |\overline{MA}|$ is the constant path length and A_1, A_2, and A_3 are the GO spreading factors corresponding

to the trajectories $\overline{OS}$, $\overline{SM}$, and $\overline{MA}$, respectively (see Fig. 8). As the feed radiation is spherical

$$A_1 = \frac{1}{|\overline{OS}|} = \frac{1}{r_F}. \tag{19}$$

The spreading factor

$$A_2 = \sqrt{\frac{\rho_1}{\rho_1 + |\overline{SM}|}}\sqrt{\frac{\rho_2}{\rho_2 + |\overline{SM}|}} \tag{20}$$

corresponds to the astigmatic wavefront leaving the subreflector, where ρ_1 and ρ_2 are the wavefront principal radii just after S, corresponding to the caustics at P and T, respectively (see Fig. 8). $\rho_1(\rho_2)$ is negative if the corresponding caustic $P(T)$ is located below the subreflector (i.e., after S, along the ray path). Finally, A_3 refers to the cylindrical wavefront after M

$$A_3 = \sqrt{\frac{\rho_3}{\rho_3 + |\overline{MA}|}} = \sqrt{\frac{\rho_3}{\rho_A}}. \tag{21}$$

Once $\vec{E}_A$ and $\vec{H}_A$ are known, the equivalence principle (i.e., the aperture method) can be applied over the antenna cylindrical aperture to estimate some important radiation characteristics (efficiency, directivity, etc.), as far as $W_A \gg \lambda$.

In the present work, the adopted feed for the efficiency analyses is a coaxial horn with external and internal aperture radii R_e and R_i, respectively (see Fig. 8). The feed radiation is provided by the corresponding TEM mode for an azimuthally-uniform coverage with vertical polarization [5], [8]–[10]. In this case, assuming a uniform phase distribution over the horn's aperture at a perfect electric conductor plane, the equivalence principle can be used to establish the following approximation for $\vec{E}_F$ [13]:

$$\begin{aligned} F(\theta_F) &= [J_0(kR_i \sin\theta_F) - J_0(kR_e \sin\theta_F)]/\sin\theta_F \\ P(\theta_F) &= 0 \end{aligned} \tag{22}$$

where $J_0(x)$ is the zero-th order Bessel function. Nevertheless, if ones adopts a TM_{01} conical horn for vertical polarization, as in [4], [6], [7], then $P(\theta_F) = 0$ and $F(\theta_F)$ is approximately given by (13) of [14], with $m = 0$ and $n = 1$. Furthermore, a TE_{01} conical horn can be adopted for horizontal polarization [6]. If so, $F(\theta_F) = 0$ and $P(\theta_F)$ is approximately given by (11) of [14], with $m = 0$ and $n = 1$.

V. Efficiency Performance

A parametric study was conducted to determine the highest possible (aperture) efficiencies among several classical omnidirectional dual-reflector antennas. The analyses were based on the aperture method discussed in Section IV. The aperture efficiency (ϵ_{ap}) considered here just accounts for the subreflector spillover [based on (17) and $|\theta_E|$] and the aperture taper efficiency (with respect to a uniform cylindrical aperture with the same W_A and ρ_A). For this purpose, it is useful to point out that the maximum directivity at $\theta = 90°$ (θ is the observation angle with respect to the z-axis, as indicated in Fig. 8) of the uniform cylindrical aperture is given by [8]

$$D_o = \frac{k^2 \rho_A W_A}{2}[|J_0(k\rho_A)|^2 + |J_1(k\rho_A)|^2]. \tag{23}$$

Due to the adopted GO principles, similar antennas (i.e., antennas with the same angular dimensions) have the same ϵ_{ap} if the same feed illumination is provided [i.e., the same $F(\theta_F)$ and $P(\theta_F)$ in (17)]. So, one of the input geometrical parameters can be set to a constant (as a dimension reference) and the choice was $W_A = 10\lambda$. The fed radiation is that of a TEM coaxial horn, approximately modeled by (22). In all cases investigated $R_e \leq 1\lambda$ (see Fig. 8); so, $D_B = 2\lambda$, aiming compact geometries (the antenna volume increases with D_B, as one can infer from Figs. 1–4). For such a small coaxial aperture the phase center of the far-field radiation is practically located at the horn's aperture. For this reason $z_B = 0$, placing the horn's aperture in the plane of the main-reflector central hole (see Fig. 8), which is a practical arrangement. So, the input values of $2\lambda \leq V_S \leq 30\lambda$ and $15\lambda \leq D_M \leq 50\lambda$ were left as the variables of the parametric study, together with R_e and R_i of the coaxial horn (see Fig. 8). Note that those are the input values adopted in Section II and, consequently, some of the geometrical features of the antennas are delineated in Figs. 5 and 6. Finally, it should be pointed out that the feed model of (22) is not practical for a large $|\theta_E|$. So, one should consider the results to be shown with care whenever $|\theta_E| \to 90°$. The corresponding θ_E values are those in Figs. 5(a) and 6(a).

With the input parameters settled, the study was conducted as follows. For a given triplet (V_S, D_M, R_e), R_i was varied ($0 < R_i < R_e$) to establish the highest ϵ_{ap} for that triplet. Several values of $R_e \leq 1\lambda$ were considered for this task, but it turned out that the maximum ϵ_{ap} values do not vary significantly with R_e for $0.7\lambda \leq R_e \leq 1\lambda$. So, just the results for $R_e = 0.9\lambda$ are depicted in Figs. 9 and 10 for the OADC/OADG and OADE/OADH, respectively. From the results one observes that the OADC is the most efficient among the configurations considered in the present investigation, achieving maximum ϵ_{ap} values of about 82%. Actually, Figs. 9 and 10 indicate that all configurations tend to achieve maximum efficiencies as $|\theta_E| \to 90°$; but one should observe that the feed model of (22) is not practical for $|\theta_E| > 80°$. The results also indicate that the OADG and OADH yielding large ϵ_{ap} values are not geometrically compact, when compared against their OADC and OADE counterparts.

The OADC geometries with the highest ϵ_{ap} values for $R_e = 0.7\lambda, \ldots, 1\lambda$ are listed in Table I, where $W_A = 10\lambda, D_B = 2\lambda$, and $z_B = 0$. From it one verifies that the optimum OADC antennas fed by TEM coaxial horns have $D_M \approx 35\lambda$ and $V_S \approx 4.6\lambda$, yielding cylindrical volumes of about $14 \times 10^3\lambda^2$.

VI. OADC Case Study

To illustrate the usefulness of the closed-form design equations of Section II and of the analysis based on the aperture method (ApM) presented in Sections IV and V, one of the OADC antennas of Table I, (more precisely, the one with $R_e = 0.9\lambda$) was analyzed by the ApM and also by the method of moments (MoM), based on [15]. Given the input parameters $W_A = 10\lambda, V_S = 4.69\lambda, D_M = 34.6\lambda, D_B = 2\lambda$, and $z_B = 0$, from (1)–(8) one readily obtains the conic parameters $F = 6.34\lambda, e = 2.4239, 2c = 15.84\lambda$, and $\beta = -8.5°$ (the values of R_i, D_S, and θ_E are those in Table I). A scale view of

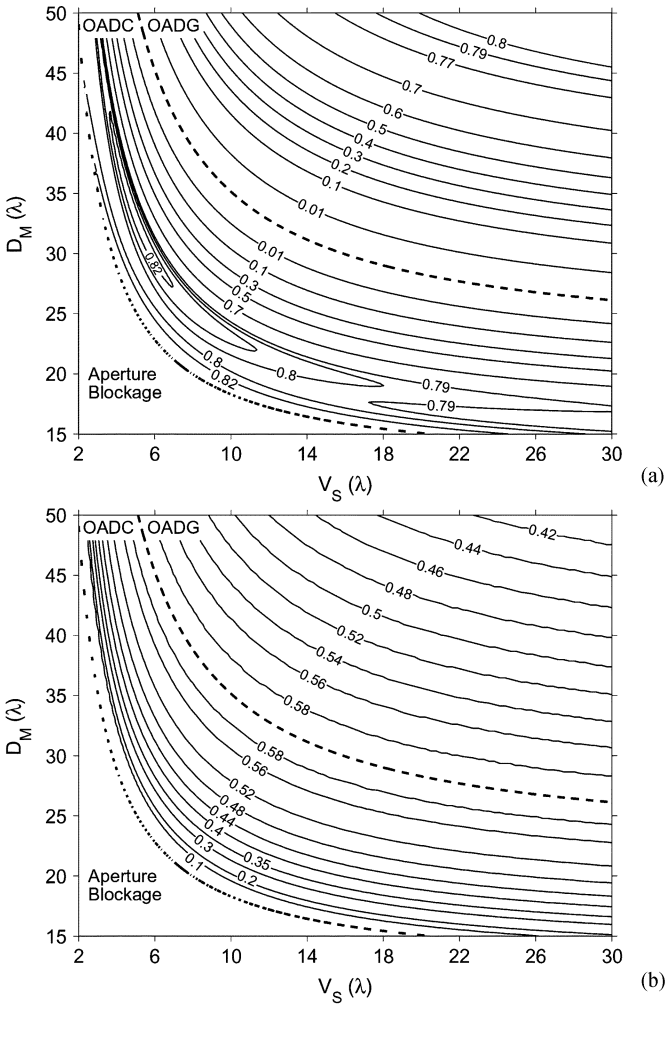

Fig. 9. Maximum aperture efficiencies of the OADC and OADG as functions of V_S and D_M, for $W_A = 10\lambda, D_B = 2\lambda, z_B = 0, R_e = 0.9\lambda$, and optimized values of $R_i < R_e$: (a) maximum efficiencies and (b) the corresponding values of R_i.

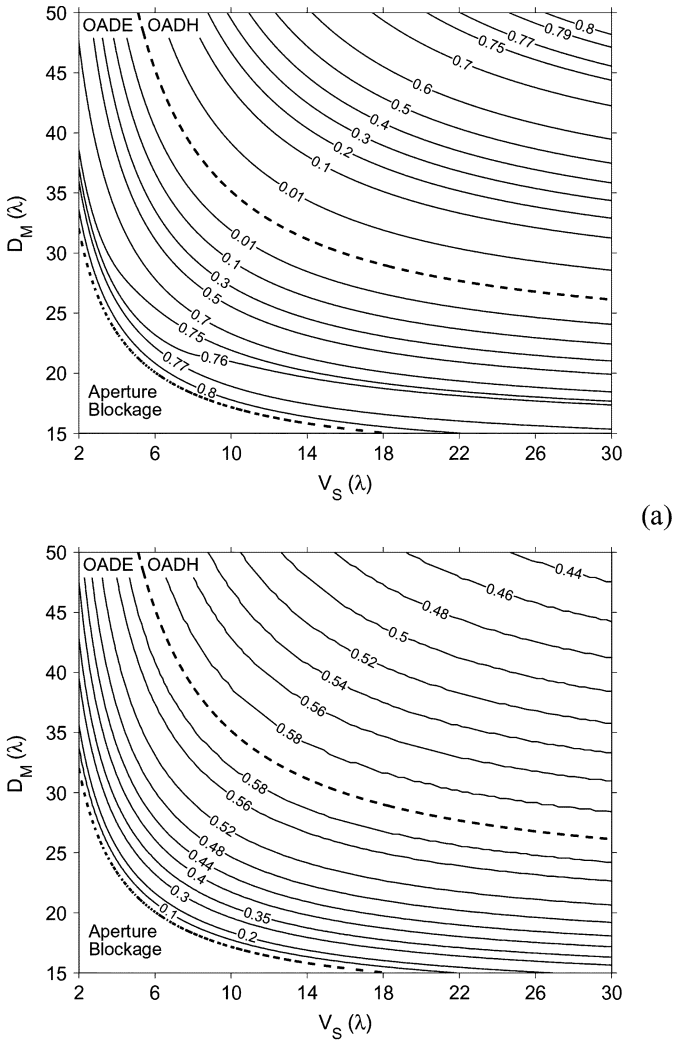

Fig. 10. Maximum aperture efficiencies of the OADE and OADH as functions of V_S and D_M, for $W_A = 10\lambda, D_B = 2\lambda, z_B = 0, R_e = 0.9\lambda$, and optimized values of $R_i < R_e$: (a) maximum efficiencies and (b) the corresponding values of R_i.

the antenna is depicted in Fig. 11(a), together with the adopted coaxial horn (for the proper MoM analysis). The horn departs from a coaxial waveguide with internal and external radii of 0.4λ and 0.7λ, respectively. The external radius is increased up to 0.9λ by means of a flare angle of 11.3°, sufficiently small to allow the use of (22) in the ApM analysis. Fig. 11(b) depicts the feed radiation pattern given by (22) and by the MoM analyses of the feed alone and of the $\text{feed} + \text{main}-\text{reflector}$ (i.e., without the subreflector), from which one observes the appropriateness of (22) for $0 \leq \theta_F \leq \theta_E = 55.1°$. In Fig. 11 the directivities are with respect to the radiated power obtained by the corresponding method/model.

The OADC radiation pattern was calculated via the ApM (discussed in Section IV) and the MoM (including all the electromagnetic couplings among the feed and reflectors). The results are depicted in Fig. 11(c) and some pertinent radiation characteristics of the main beam are detailed in Table II. From the results one observes that, except for the main-beam direction (θ_o in Table II), the ApM is capable of estimating with reasonable accuracy the main-beam radiation characteristics for classical omnidirectional antennas with moderately large aperture widths (W_A). That should come with no surprise for the OADC (and also for the OADE), as such antenna is (geometrically) free of blockage mechanisms [see, for instance, Fig. 11(a)].

The main-beam deviation estimated by the MoM analysis is due to the proximity between the horn's aperture and the subreflector, which precludes the desired spherical illumination of the subreflector. This fact ultimately causes an almost linear perturbation of the phase distribution over the antenna's cylindrical aperture, thus deviating the main beam from the expected $\theta = 90°$. This phase perturbation can be slightly compensated by adjusting the value of z_B (see Fig. 8). Although the results are not shown here, a new OADC configuration was designed with the same input parameters, except for $z_B = 0.16\lambda$ (i.e., the principal focus O was placed inside the horn, 0.16λ away from the horn's aperture, according to the notation in Fig. 8). The MoM analysis further indicated that the main beam now has its maximum around $\theta = 90°$, with minor variations of the remaining main-beam radiation characteristics with respect to the results in Table II.

TABLE I
OADC GEOMETRIES (FED BY A TEM COAXIAL HORN) FOR MAXIMUM APERTURE EFFICIENCY ($\epsilon_{\rm ap}$), WITH $W_A = 10\lambda$, $D_B = 2\lambda$, AND $z_B = 0$

Coaxial Horn		OADC Dual-Reflector System				Aperture
R_e	R_i	V_S	D_M	D_S	θ_E	Efficiency ($\epsilon_{\rm ap}$)
0.7λ	0.55λ	4.36λ	35.4λ	13.0λ	58.4°	82.6%
0.8λ	0.47λ	4.49λ	35.0λ	12.9λ	57.4°	82.5%
0.9λ	0.40λ	4.69λ	34.6λ	12.6λ	55.1°	82.4%
1.0λ	0.35λ	4.90λ	34.3λ	12.2λ	52.5°	82.2%

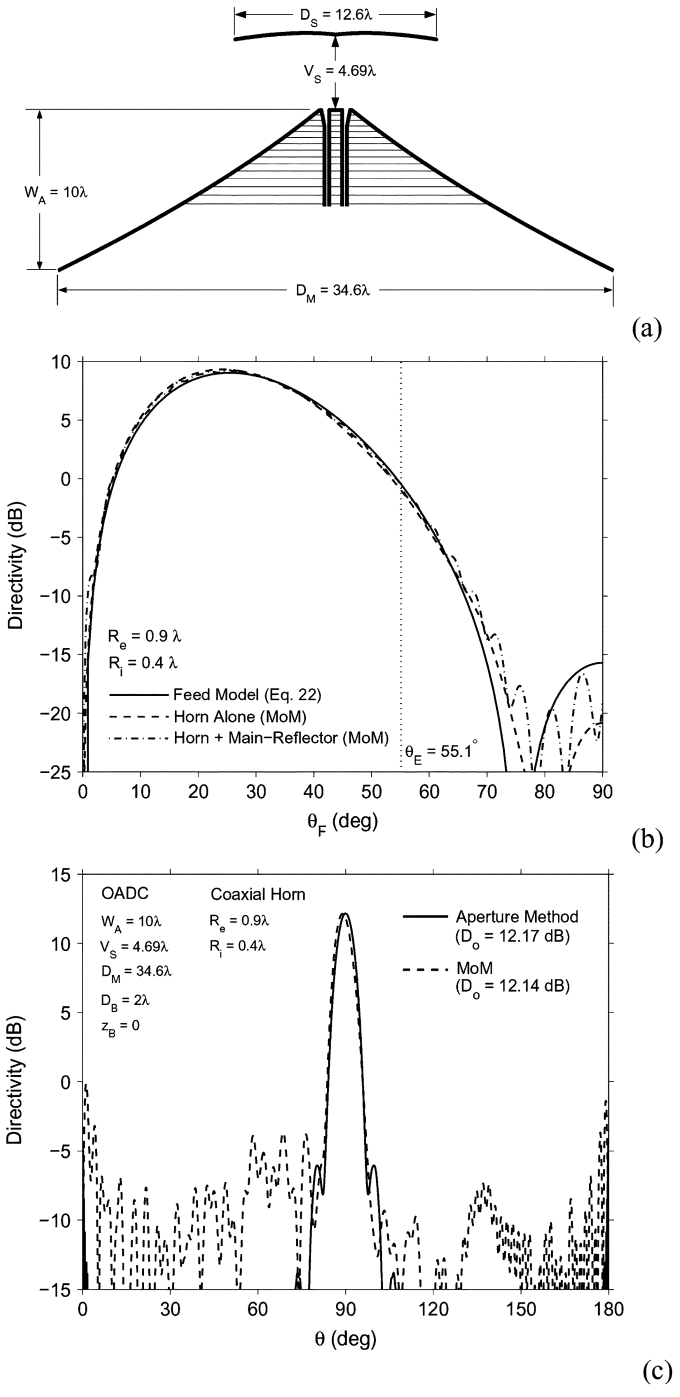

Fig. 11. Radiation characteristics of the OADC with $W_A = 10\lambda, D_B = 2\lambda, z_B = 0, D_M = 34.6\lambda$, and $V_S = 4.69\lambda$, fed by a TEM coaxial horn with $R_e = 0.9\lambda$ and $R_i = 0.4\lambda$: (a) scale view, (b) feed radiation pattern, and (c) OADC radiation pattern.

TABLE II
RADIATION CHARACTERISTICS OF THE OADC OF FIG. 11

Analysis	D_o(dB)	θ_o	HPBW	$\epsilon_{\rm ap}$
ApM	12.17	90°	6.4°	82.4%
MoM	12.14	89°	6.2°	81.9%

VII. CONCLUSION

Closed-form equations for the design of any classical dual-reflector antennas with omnidirectional radiation characteristics were presented, based on GO principles. Such principles were also adopted to derive the vector field at the antenna's cylindrical aperture, allowing the approximate use of the aperture method to estimate some important main-beam radiation characteristics. The hole formulation enabled a general parametric study, involving several possible classical configurations, in order to determine some rules-of-thumb for the specification of compact dual-reflector arrangements and also of highly efficient configurations (in this case, fed by a TEM coaxial horn). Basically, the study determined that the OADE configuration provides the most compact arrangements, but the OADC is the one capable of yielding the most efficient antennas. The formulation was further applied to the synthesis and analysis of a highly efficient OADC antenna. The results were compared against those provided by the MoM analysis, which demonstrated that the suggested formulation and the corresponding results are useful for antennas with moderately large aperture widths.

REFERENCES

[1] W. V. T. Rusch, "The current state of the reflector antenna art—Entering the 1900's," *Proc. IEEE*, vol. 80, no. 1, pp. 113–126, Jan. 1992.
[2] E. Willoughby and E. Heider, "Laboratory development notes—Omnidirectional vertically polarized paraboloid antenna," *IEEE Trans. Antennas Propag.*, vol. 7, no. 2, pp. 201–203, Apr. 1959.
[3] Y. Takeichi and T. Katagi, "The omnidirectional horn-reflector antenna," in *Proc. IEEE Antennas Propag. Soc. Int. Symp.*, 1970, pp. 40–47.
[4] A. P. Norris and W. D. Waddoup, "A millimetric wave omnidirectional antenna with prescribed elevation shaping," in *Proc. ICAP—4th Int. Conf. Antennas and Propagation*, 1985, pp. 141–145.
[5] M. Orefice and P. Pirinoli, "Dual reflector antenna with narrow broadside beam for omnidirectional coverage," *Electron. Lett.*, vol. 29, no. 25, pp. 2158–2159, Dec. 9, 1993.
[6] P. Besso, R. Bills, P. Brachat, and R. Vallauri, "A millimetric wave omnidirectional antenna with cosecant squared elevation pattern," in *Proc. ICAP 10th Int. Conf. Antennas and Propagation*, vol. 1, 1997, pp. 448–451.
[7] H. B. Abdullah, "A prototype Q-band antenna for mobile communication systems," in *Proc. ICAP 10th Int. Conf. Antennas and Propagation*, vol. 1, 1997, pp. 452–455.
[8] A. G. Pino, A. M. A. Acuña, and J. O. R. Lopez, "An omnidirectional dual-shaped reflector antenna," *Microw. Opt. Tech. Lett.*, vol. 27, no. 5, pp. 371–374, Dec. 5, 2000.
[9] J. R. Bergmann, F. J. V. Hasselmann, and M. G. C. Branco, "A single-reflector design for omnidirectional coverage," *Microw. Opt. Tech. Lett.*, vol. 24, no. 6, pp. 426–429, Mar. 20, 2000.
[10] J. R. Bergmann and F. J. S. Moreira, "An omni directional ADE reflector antenna," *Microwave Opt. Tech. Lett.*, vol. 40, no. 3, pp. 250–254, Feb. 5, 2004.
[11] F. J. S. Moreira and A. Prata Jr., "Generalized classical axially symmetric dual-reflector antennas," *IEEE Trans. Antennas Propag.*, vol. 49, no. 4, pp. 547–554, Apr. 2001.
[12] G. A. Deschamps, "Ray techniques in electromagnetics," *Proc. IEEE*, vol. 60, no. 9, pp. 1022–1035, Sep. 1972.
[13] R. F. Harrington, *Time-Harmonic Electromagnetic Fields*, New York: McGraw Hill, 1961.

[14] S. Silver, Ed., *Microwave Antenna Theory and Design*, New York: McGraw Hill, 1949, ch. 10.
[15] F. J. S. Moreira, "Design and rigorous analysis of generalized axially-symmetric dual-reflector antennas," Ph.D. dissertation, Univ. Southern California, Los Angeles, 1997.

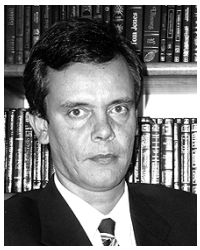

Fernando José da Silva Moreira (S'89–M'98) was born in Rio de Janeiro, Brazil, in 1967. He received the B.S. and M.S. degrees in electrical engineering from the Catholic University, Rio de Janeiro, in 1989 and 1992, respectively, and the Ph.D. degree in electrical engineering from the University of Southern California, Los Angeles, in 1997.

Since 1998, he has been with the Department of Electronics Engineering of the Federal University of Minas Gerais, Brazil, where he is currently an Associate Professor. His research interests are in the areas of electromagnetics, antennas and propagation. He has authored or coauthored over 60 journal and conference papers in these areas.

Dr. Moreira is a Member of Eta Kappa Nu and the Brazilian Microwave and Optoelectronics Society.

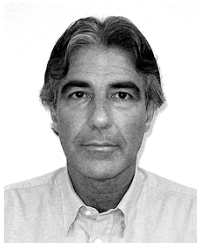

José Ricardo Bergmann (M'89) received the degree of electrical engineer from Universidade Federal do Rio Grande do Sul, Brazil, in 1975, the M.Sc. degree in electrical engineering from Instituto Militar de Engenharia, Brazil, in 1979, and the Ph.D. degree in electrical engineering from Queen Mary College, University of London, London, U.K., in 1986.

He is an Associate Professor at the Catholic University of Rio de Janeiro, Rio de Janeiro, Brazil, where he is also the Head of the Antenna Group of the Center of the Telecommunications Studies (CETUC). Since 1998, he is also Associate Vice President for Academic Affairs-Research and Post Graduate Programs of the Catholic University of Rio de Janeiro. His research interests comprise numerical modeling, synthesis and analysis of reflector systems.

Dr. Bergmann was Vice President and President of the Brazilian Microwave and Optoelectronics Society (SBMO) from 1996 to 2000.